$$\mathbf{B}=\begin{bmatrix}1/L_1 & 0 & 0 & 0 & 0 & 0\\ 0 & 1/L_1 & 0 & 0 & 0 & 0\end{bmatrix}^T,\ \mathbf{C}=\begin{bmatrix}0 & 0 & 0 & 0 & 1 & 0\\ 0 & 0 & 0 & 0 & 0 & 1\end{bmatrix}$$

$$\mathbf{B}_d=\begin{bmatrix}0 & 0 & 0 & 0 & -1/L_2 & 0\\ 0 & 0 & 0 & 0 & 0 & -1/L_2\end{bmatrix}^T.$$

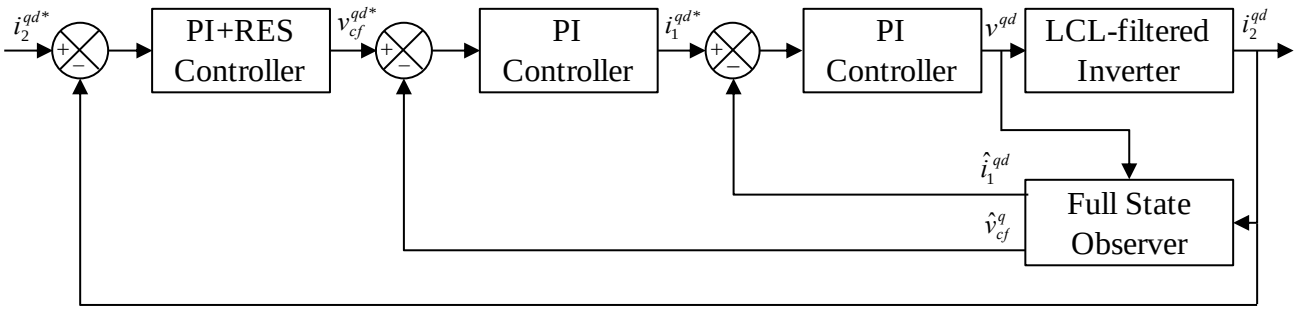

Figure 2. Overall Block Diagram of the Proposed Control Scheme

The state-space equations in (10) and (11) can be discretized by using a zero-order hold (ZOH) as

$$\mathbf{x}(k+1)=\mathbf{G}\mathbf{x}(k)+\mathbf{H}\mathbf{u}(k)+\mathbf{H}_d\mathbf{w}(k) \quad (12)$$

$$\mathbf{y}(k)=\mathbf{C}\mathbf{x}(k) \quad (13)$$

where $\mathbf{G}$, $\mathbf{H}$, and $\mathbf{H}_d$ denote the discrete-time representation of matrices in the state equations (10) and (11) [15].

Proposed Control Scheme

To provide the inverter output voltage in the event of operation mode transition, the proposed control scheme consists of three cascaded control loops which are composed of the grid-side current control loop, capacitor voltage control loop, and inverter-side current control loop. The control of each of these control loops is accomplished by a separate controller. Since the inverter has to operate as a voltage source in the islanded mode, the grid-side current control loop becomes inactive in this operation mode. Thus, only the capacitor voltage controller and inverter-side current controller are used in the islanded mode. To implement both the capacitor voltage controller and inverter-side current controller, the traditional PI controllers are employed as follows:

$$G_{PI}(s)=\frac{K_p s+K_I}{s} \quad (14)$$

where K_P and K_I are the proportional and integral gains, respectively

For the purpose of digital implementation, the transfer function of the PI controller can be discretized by using the bilinear transformation as

$$G_{PI}(z)=\frac{1}{2}\frac{(2K_p+K_i)z+K_iT_s-2K_p}{z-1}. \quad (15)$$

where T_s is the sampling period of the controller.

Apart from the reference tracking capability of the controller, the grid-side current controller is required to maintain a low harmonic distortion level of the injected current under the presence of harmonically distorted grid voltages. In general, the grid voltage is composed of a fundamental component and harmonic components. In the SRF, the fundamental grid voltages are transformed into constant values which can be easily dealt with by using the PI controller. On the contrary, the harmonic components of the grid voltage still vary sinusoidally with time in the SRF. To suppress these sinusoidally-varying disturbances effectively, resonant control is introduced. The resonant control can be incorporated into the traditional PI controller to constitute PI+RES controller. The resonant control terms can be expressed as

$$G_{RES}(s)=\frac{2K_{RESi}\omega_{ci}s}{s^2+2\omega_{ci}+\omega_i^2} \quad (16)$$

where $i=6k\pm1$ denotes the order of the harmonics which three-phase grid voltages include, k is a positive integer, K_{RESi} is the resonant control gain, ω_{ci} is the cut-off frequency, and ω_i is the resonant frequency. Transfer function in (16) can be discretized by using the bilinear transformation as

$$G_{RES}(z)=\frac{a_2z^2+a_1z^1+a_0}{b_2z^2+b_1z^1+b_0} \quad (17)$$

where $a_2=4K_{res}T_s\omega_{ci}$, $b_2=T_s^2\omega_i^2+2\omega_{ci}T_s^2+4$, $a_1=0$
$b_1=2T_s^2\omega_i^2+4T_s^2\omega_{ci}-8$, $a_0=-4K_{res}T_s\omega_{ci}$
$b_0=T_s^2\omega_i^2+2T_s^2\omega_c+4$.

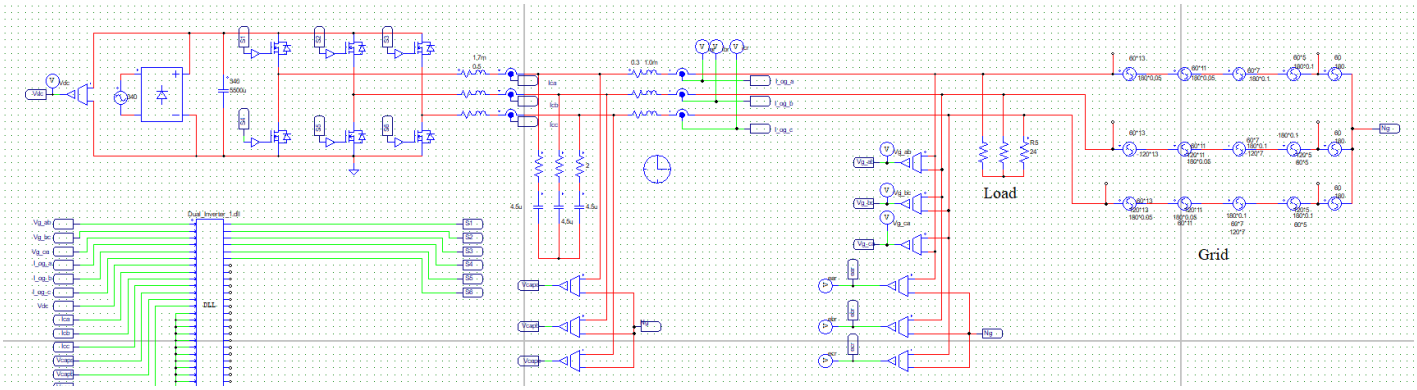

Figure 3. Simulation Configuration for a Grid-connected Inverter System

In three-phase system, the harmonic components in three-phase grid voltages exist in the order of $i = 6k \pm 1$, namely, in the orders of the 5th, 7th, 11th, and 13th. Thus, the proposed control scheme is designed by considering that three-phase grid voltages consist of the fundamental term and the harmonic terms in the orders of the 5th, 7th, 11th, and 13th. As a result of using the Park's transformation, these harmonic disturbances become the harmonic components in the orders of the 6th and 12th in the SRF. By taking these two main harmonic terms into account, the PI+RES controller for the grid-side current control loop can be given as

$$G_{PI+RES}(z) = G_{PI}(z) + G_{RES6}(z) + G_{RES12}(z). \qquad (18)$$

Generally, to realize a seamless transfer algorithm or indirect current control scheme for a grid-connected inverter, all the inverter state variables such as the grid-side currents, capacitor voltages, and inverter-side currents should be measured. However, such a realization as in the conventional works is neither acceptable nor adequate any longer because it unpractically increases the total cost of inverter systems as well as the implementation complexity of digital controller.

To alleviate this limitation, a state estimation approach is introduced in this paper, which significantly reduces the system cost by eliminating the requirement of additional number of sensors in implementing the proposed control structure. For this purpose, a full-state observer is used in the discrete-time domain. As a result, by estimating the capacitor voltages and inverter-side currents by the full-state observer, the proposed control structure can be achieved by using only the measurements of grid-side currents. A full-state observer which estimates the capacitor voltages and inverter-side currents can be constructed in the discrete-time domain as

$$\hat{\mathbf{x}}(k+1) = \mathbf{G}\hat{\mathbf{x}}(k) + \mathbf{H}\mathbf{u}(k) + \mathbf{H}_d\mathbf{w}(k) + \mathbf{L}(\mathbf{y}(k) - \mathbf{C}\hat{\mathbf{x}}(k)) \qquad (19)$$

where the symbol "^" denotes the estimated quantities and **L** is the observer gain vector. The entire block diagram of the proposed control scheme is shown in Fig. 2.

Comparative Simulation Results

To validate the usefulness of the proposed control scheme, the comparative simulations have been carried out using the PSIM software. The simulation model for an LCL-filtered grid-connected inverter is constructed as depicted in Fig. 3. The main controllers are implemented by using the PSIM DLL block.

To verify the robustness of the proposed control scheme against the abnormal grid environment, the harmonically distorted grid voltages are added to the ideal grid voltages. The entire distorted grid voltages are formed by adding 10% of the 5th and 7th harmonic components with respect to the nominal grid voltage, and 5% of the 11th and 13th harmonic components with respect to the nominal grid voltage into the ideal grid. For performance comparison, the conventional indirect current control scheme [7] and the enhanced indirect current control scheme [14] are employed to highlight the superior performance of the proposed control scheme.

Fig. 4 shows the simulation results of the conventional indirect current control scheme under the ideal grid voltages. As can be observed from Fig. 4(b), the conventional indirect current controller provides reasonably sinusoidal steady-state current waveforms. Moreover, Fig. 4(c) through Fig. 4(e) shows considerably stable capacitor voltage responses and fast transient current responses under a step change in reference current.

Fig. 5 shows the simulation results of the conventional indirect current control scheme under distorted grid voltages as given in Fig. 5(a). As opposed to the phase-current waveforms in Fig. 4(b), the steady-state responses of grid-side currents are severely distorted due to the adverse grid voltages as shown in Fig. 5(b), even though the transient responses are similar to Fig. 4. These harmful distortions can be also observed in the Fig. 5(c), Fig. 5(d), and Fig. 5(e).

Fig. 6 shows the simulation results for the enhanced multiloop control scheme presented in [14] under the same distorted grid conditions as in Fig. 5(a). As can be clearly seen from Fig. 6(b), the grid-side three-phase current waveforms remain quite sinusoidal regardless of highly distorted grid voltage. Moreover, Fig. 6(c) and Fig 6(e) reveal that the existing enhanced multiloop control scheme still provides fast and stable transient responses. It is worth mentioning that the inverter-side currents and capacitor voltages are distorted due to the distorted grid voltage. However, these distortions do not influence the grid-side currents. As a result, the simulation

results in Fig. 6 confirm that the existing enhanced multiloop control scheme [14] can provide better control performance than that of the conventional indirect current control scheme.

To highlight the usefulness of the proposed control scheme, Fig. 7 shows the simulation results of the proposed scheme under the same distorted grid voltages. As can be seen from Fig. 7, the proposed control scheme can give a similar control performance with that of the existing enhanced multiloop control scheme in [14] even though the proposed control scheme only employs the grid-side current sensors instead of measuring all the system states as in the conventional approaches. This fact well confirms the validity and usefulness of the proposed control structure.

Fig. 8 shows the FFT results of *a*-phase current for three control schemes under the same distorted grid voltages. As can be observed, the inability of the conventional indirect current control scheme to deal with sinusoidal disturbances leads to considerably high total harmonic distortion (THD) level of injected current as shown in Fig. 8(a). On the other hand, as shown in Fig. 8(b) and Fig. 8(c), the enhanced indirect current control method and the proposed control scheme produce lower THD levels in the injected current even under heavily distorted grid voltages. The THD values in Fig. 8(b) and Fig. 8(c) indicate the good control performance of the proposed control scheme even if only grid-side current sensors are used in the proposed scheme.

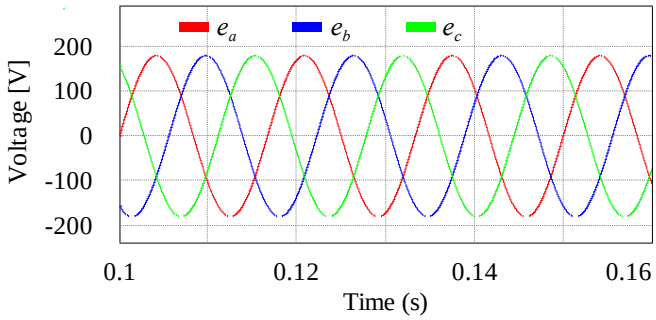

(a) Three-phase grid voltages

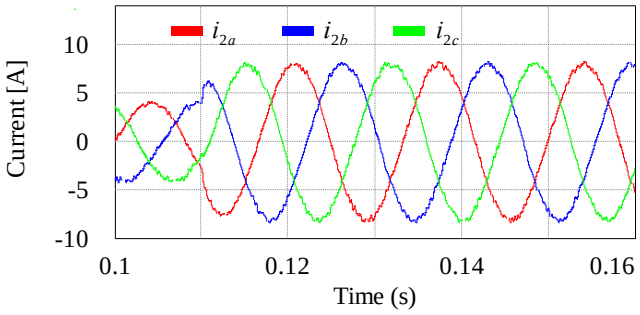

(b) Three-phase grid-side currents

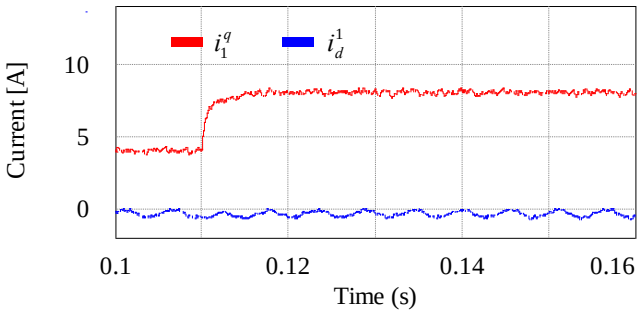

(c) Inverter-side currents in the SRF

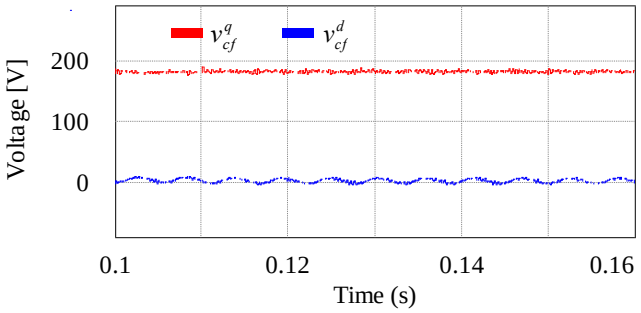

(d) Capacitor voltages in the SRF

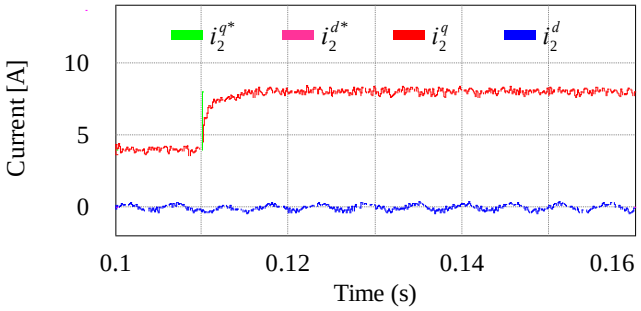

(e) References and grid-side currents in the SRF

Figure 4. Simulation Results of the Conventional Indirect Current Control Scheme under the Ideal Grid Voltage

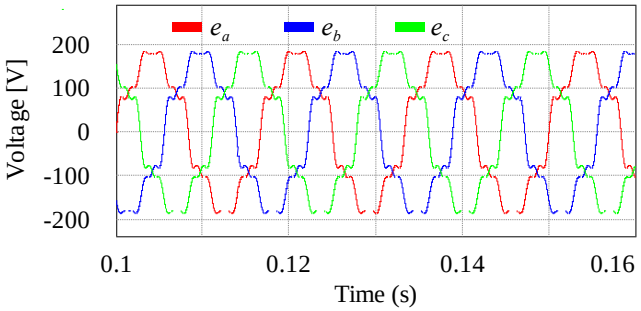

(a) Three-phase grid voltages

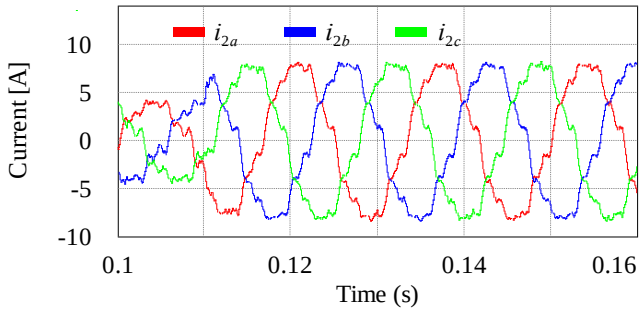

(b) Three-phase grid-side currents

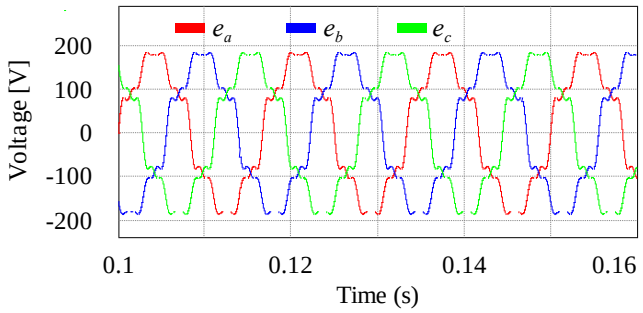

(a) Three-phase grid voltages

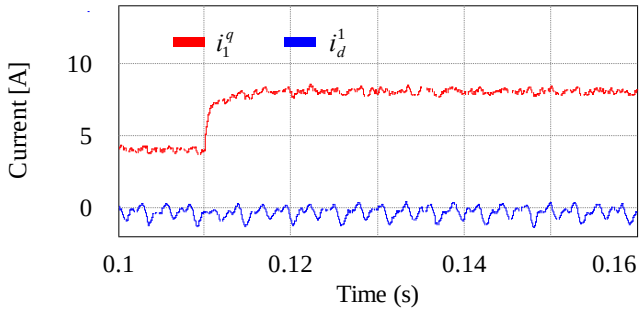

(c) Inverter-side currents in the SRF

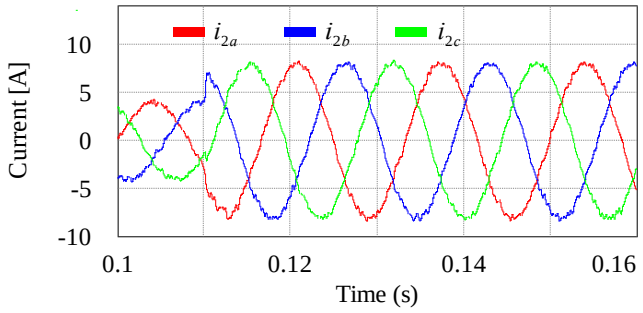

(b) Three-phase grid-side currents

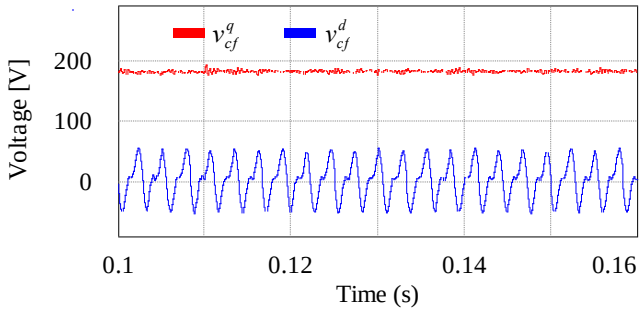

(d) Capacitor voltages in the SRF

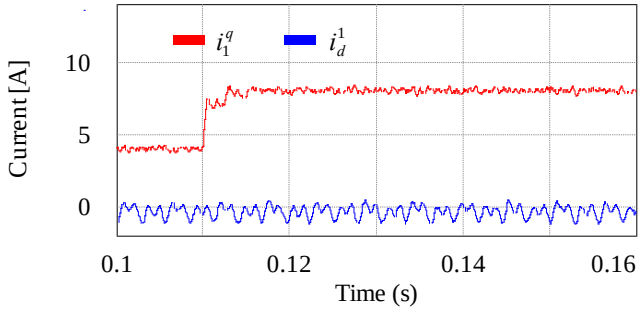

(c) Inverter-side currents in the SRF

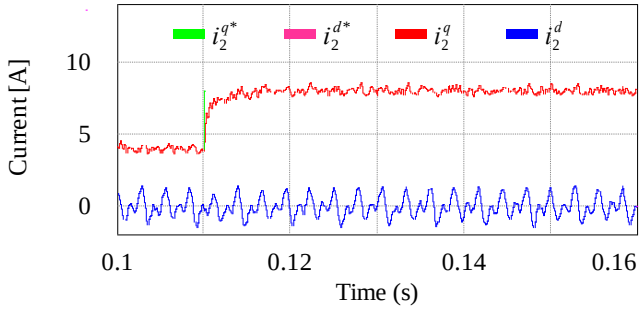

(e) References and grid-side currents in the SRF

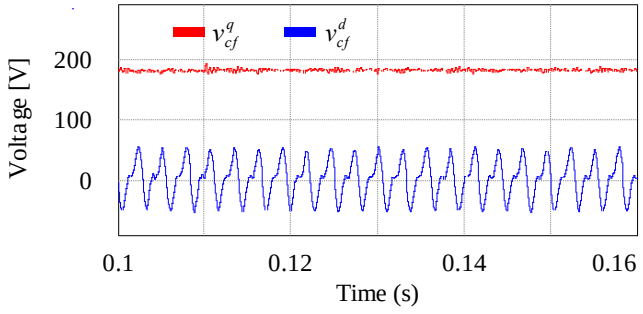

(d) Capacitor voltages in the SRF

Figure 5. Simulation Results of the Conventional Indirect Current Control Scheme under Distorted Grid Voltages

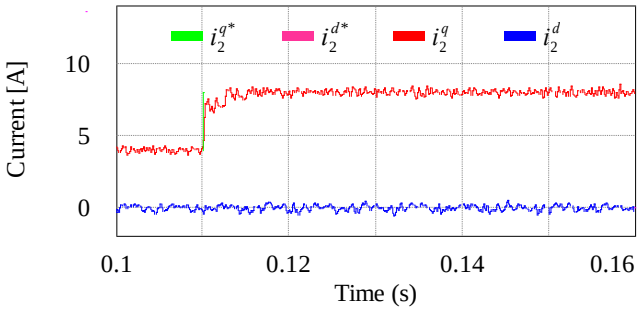

(e) References and grid-side currents in the SRF

Figure 6. Simulation Results of the Enhanced Indirect Control under Distorted Grid Voltages

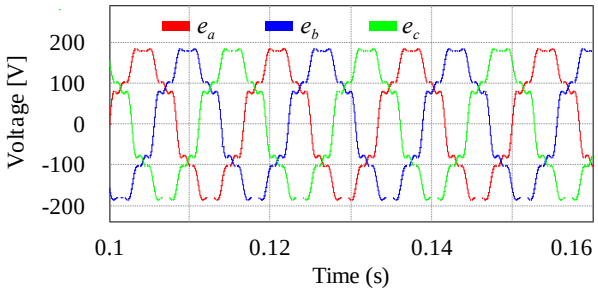

(a) Three-phase grid voltages

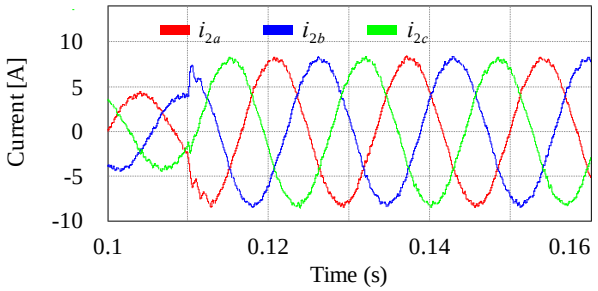

(b) Three-phase grid-side currents

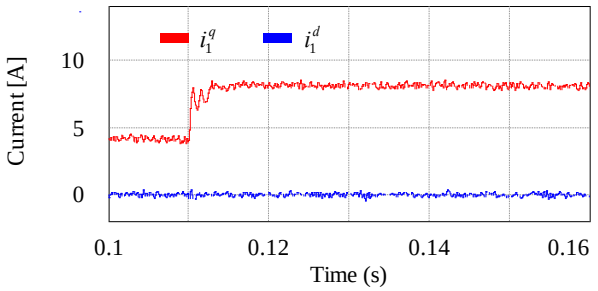

(c) Inverter-side currents in the SRF

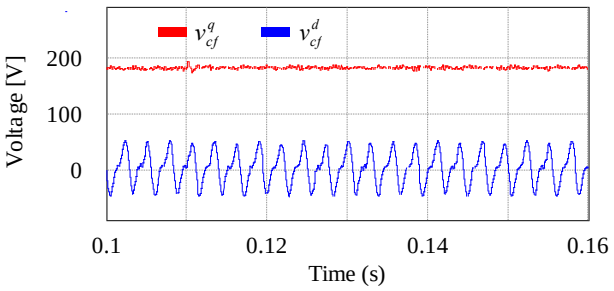

(d) Capacitor voltages in the SRF

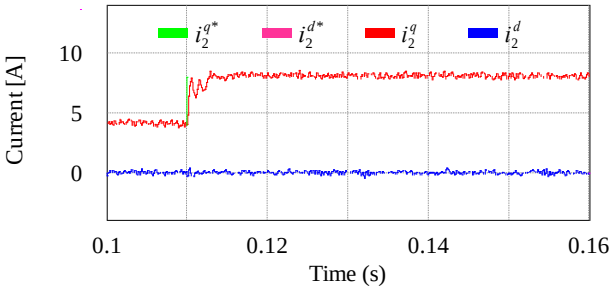

(e) References and grid-side currents in the SRF

Figure 7. Simulation Results of the Proposed Control Scheme under Distorted Grid Voltages

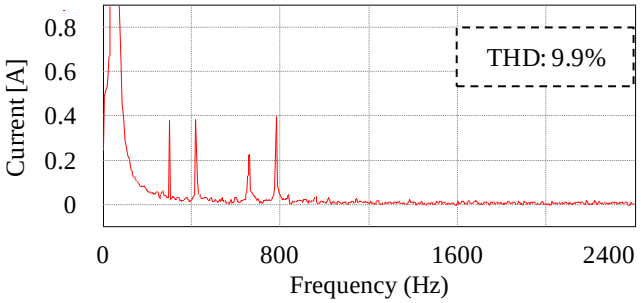

(a) Conventional indirect current control scheme under distorted grid voltages

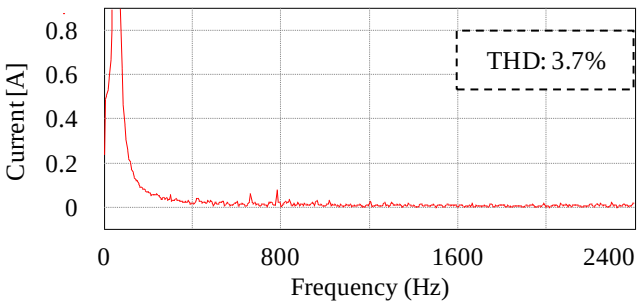

(b) Enhanced indirect current control scheme under distorted grid voltages

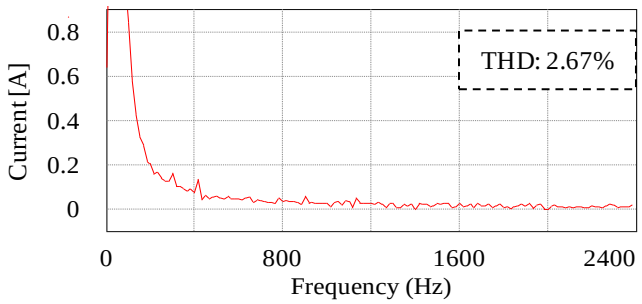

(c) Proposed control scheme under distorted grid voltages

Figure 8. FFT Results of Grid-side *a*-phase Current

CONCLUSION

Conventionally, the multiloop and indirect current control schemes have been used to cope with the unexpected transient voltages supplied to critical loads. However, the capacitor voltage and inverter-side currents should be also measured in these control strategies in addition to the measurements of grid-side currents. This requirement unpractically increases the total cost of inverter systems as well as the implementation complexity of DG systems. To address this problem, a simple design and implementation method of an indirect current control for LCL-filtered grid-connected inverter is presented by using reduced number of sensors. The proposed control scheme mainly consists of an indirect current controller and a full-state observer. For the purpose of enhancing the disturbance rejection capability, a PI+RES controller is employed in the outer loop of the indirect current controller, while two PI controllers are used in the inner loops in a cascaded structure. The full-state observer is used to estimate the capacitor voltages and inverter-side currents in the discrete-time domain. As a consequence, the indirect current controller can be accomplished by using only the measurements of grid-side currents. Theoretical analyses and comparative simulation results have been provided to confirm the usefulness of the proposed control scheme.

ACKNOWLEDGEMENTS

This study was supported by the Research Program funded by the SeoulTech (Seoul National University of Science and Technology).

REFERENCES

[1] J. de Matos, F. e Silva, and L. Ribeiro, “Power control in AC isolated microgrids with renewable energy sources and energy storage systems,” IEEE Trans. Ind. Electron., vol. 62, no. 6, pp. 3490–3498, Jun. 2014.

[2] H. Han, X. Hou, J. Yang, J. Wu, M. Su, and J. M. Guerrero, “Review of power sharing control strategies for islanding operation of AC microgrids,” IEEE Trans. Smart Grid, vol. 7, no. 1, pp. 200–215, Jan. 2016.

[3] O. C. Montero-Hernández and P. N. Enjeti, “Ride-through for critical loads,” IEEE Ind. Appl. Mag., vol. 8, no. 6, pp. 45–53, Dec. 2002.

[4] R. Tirumala, N. Mohan, and C. Henze, “Seamless transfer of grid-connected PWM inverters between utility-interactive and stand-alone modes,” APEC. Seventeenth Annual IEEE Appl. Power Electron. Conf. Expo., vol. 2, no. c, pp. 1081–1086, Mar. 2002.

[5] H. Kim, T. Yu, and S. Choi, “Indirect current control algorithm for utility interactive inverters in distributed generation systems,” IEEE Trans. Power Electron., vol. 23, no. 3, pp. 1342–1347, May 2008.

[6] Z. Yao, L. Xiao, and Y. Yan, “Seamless transfer of single-phase grid interactive inverters between grid-connected and stand-alone modes,” IEEE Trans. Power Electron., vol. 25, no. 6, pp. 1597-1603, Jun. 2010.

[7] Y. Prabowo, M. Kwon, S. Park, and S. Choi, “Improved indirect current control for utility-interactive inverter system with critical load,” 3rd Conf. on Power Engineering and Renewable Energy (ICPERE), pp. 1–5, Nov. 2016.

[8] S. Yoon, H. Oh, and S. Choi, “Controller design and implementation of indirect current control based utility-interactive inverter system,” IEEE Trans. Power Electron., vol. 28, no. 1, pp. 26–30, Jan. 2013.

[9] S. W. Kang and K. H. Kim, “Sliding mode harmonic compensation strategy for power quality improvement of a grid-connected inverter under distorted grid condition,” IET Power Electron., vol. 8, no. 8, pp. 1461-1472, Aug. 2015.

[10] H. S. Kim, J. S. Kim, and K. H. Kim, “Power quality improvement of grid connected inverter under distorted and unbalanced grid,” KIPE Journal of Power Electron., vol. 16, no. 4, pp. 1578-1586, July 2016.

[11] T. H. Nguyen and K. H. Kim, “Finite control set – model predictive control with modulation to mitigate harmonic component in output current for a grid-connected inverter under distorted grid conditions,” Energies, vol. 10, no. 7, pp. 1-25, July 2, 2017.

[12] S. J. Yoon, N. B. Lai, and K. H. Kim, “A systematic controller design for a grid-connected inverter with LCL filter using a discrete-time integral state feedback control and state observer,” Energies, vol. 11, no. 437, pp. 1-20, Feb. 2018.

[13] N. B. Lai and K. H. Kim, “Robust control scheme for three-phase grid-connected inverters with LCL-filter under unbalanced and distorted grid conditions,” IEEE Trans. on Energy Conversion, DOI: 10.1109/TEC.2017.2757042

[14] N. B. Lai and K. H. Kim, “Enhanced multiloop control scheme for an LCL-filtered grid-connected inverter under abnormal grid voltage conditions,” Inter. Journal of Applied Eng. Research, vol. 12, no. 19, pp. 8830-8837, Oct. 2017.

[15] G. F. Franklin, J. D. Powell, and M. Workman, Digital Control of Dynamic Systems, 3rd ed., California, Addison Wesley Longman, 1998.